InGaAs/AlGaInAs/InP Laser with Compressively Strained Multiquantum Well Layers for High Speed Modulation Bandwidth

M.T. Furtado[1], E.J.T. Manganote[1,2], A.C.G. Bordeaux-Rêgo[1],
F. Steinhagen[3], H. Janning[3] and H. Burkhard[3]

[1] *Centro de Pesquisa e Desenvolvimento,*
Telecomunicações Brasileiras S/A-TELEBRÁS,
C.P.1579, 13088-061 Campinas, SP, Brazil

[2] *Universidade Paulista - OBJETIVO,*
Campus Magalhães Teixeira, Av. Projetada 280,
13043-140 Campinas, SP, Brazil

[3] *Deutsche Telekom, PO Box 100003,*
64276 Damrstadt, Germany

Received April 15, 1997

The modulation frequency response of compressively strained multiquantum well (MQW) lasers grown with an InGaAs/AlGaInAs/InP heterostructure and emitting at the wavelength of 1.55μm is presented. The laser devices processed with the mushroom-stripe buried structure present a high frequency 3 dB bandwidth above 20 GHz. The frequency response was measured with the small signal modulation technique. The logarithmic subtraction method was employed to extract the intrinsic frequency response of the MQW active layer, providing the determination of important laser parameters: the differential gain, the nonlinear gain coefficient and the maximum 3 dB frequency bandwidth.

I. Introduction

Strained multiquantum well (MQW) distributed feedback (DFB) lasers are very attractive for high speed optical communications. The strain provides a reduced density of states in the valence band of the MQW active region which increases the differential gain [1,2]. The latter improves the modulation frequency bandwidth, narrows the single mode emission linewidth and lowers the emission wavelength chirp, which are important characteristics for applications in long distance optical systems [1]. We have recently reported the evaluation of the differential gain in MQW laser devices grown with InGaAs/InGaAsP/InP heterostructures utilizing threshold current density measurements [3].

The InGaAs/AlGaInAs/InP material system has been predicted to yield MQW lasers with higher frequency bandwidths due the larger conduction band offset compared to the most widely used InGaAs/InGaAsP/InP system [4]. This was confirmed with lattice matched MQW lasers where the differential gain was observed to increase with the conduction band discontinuity [5], but with a concomitant increase of the nonlinear gain coefficient. The latter is responsible for the damping of the frequency response, and consequently, limits the maximum modulation bandwidth. More recently, devices presenting a significant increase of the differential gain [6], and a frequency modulation bandwidth above 20 GHz [7] were reported with compressive strained InGaAs/InGaAlAs/InP MQW heterostructures.

In this work, we have further analysed the high speed characteristics of a compressively strained InGaAs/AlGaInAs/InP separate confinement heterostructure (SCH) MQW-DFB lasers. The high frequency response measurements were carried out using the small signal modulation technique. The parasitic contributions due the device processing structure were eliminated by performing the logarithmic subtraction of the frequency response at a lower current bias level. From this analysis we have evaluated the differential gain and the nonlinear gain coefficient of the MQW active region, as well as the maximum modulation 3dB bandwidth. In section II, we describe the growth and processing steps involved in the device fabrication, as well as the experimental procedure for the optical modulation response measurements. In section III, we present the results and the analysis for the extraction of the MQW laser intrinsic parameters. Finally, the conclusion is presented in section IV.

II. Device fabrication and experimental setup

The strained MQW active region was grown by molecular beam epitaxy on a p^+-InP substrate over a 500 Å thick Be doped p-type AlInAs buffer layer. The MQW heterostructure consists of 10 compressively strained (1.2%) 30Å thick InGaAs QW layers grown between 80Å thick AlGaInAs lattice matched barriers. The thickness and composition of the QW layers correspond to the photoluminescence peak at the wavelength of 1.55 μm. The SCH comprised two AlGaInAs waveguide layers designed asymmetrically to minimize the transport distance of the holes while maximizing the overlap between the vertically guided optical field distribution and the active region [7]. The composition of the lattice matched AlGaInAs waveguide and barrier layers correspond to the photoluminescence peak at the wavelength of 1.26 μm. The QW layers were grown Be doped with $p = 5 \times 10^{17}$ cm^{-3}. The first order DFB grating was defined on the upper AlGaInAs waveguide layer by electron beam lithography and low energy Ar^+ ion beam etching. A $2\times\lambda/8$ phase shift was included in the grating in order to minimize longitudinal hole burning effects, while the Bragg wavelength was negatively detuned by 10 nm from the gain peak. After, a 2 μm thick n-type Si doped InP layer with $n = 2\times 10^{18}$ cm^{-3} and a final thin n^+-InP contact layer were successively grown on top by metalorganic chemical vapour deposition. The devices were processed with the mushroom stripe (constricted mesa) buried structure [8]. The mesas 7 μm wide were dry etched down to the substrate, and the top layers were selectively undercut by wet etching to define an active region width of 1.2 μm. The undercut mesas were regrown with semi-insulating InP:Fe by hydride vapour phase epitaxy. The lasers were cleaved with cavity lengths of 200 μm. The threshold currents and slope efficiencies measured are in the range 11-14 mA and 0.1-0.15 W/A per facet, respectively. The DFB emission wavelength peaks are in the range 1.541- 1.546 μm, with sidemode supression ratios above 30 dB up to 6 mW optical power.

The small signal modulation response was measured with an HP 71400 electro- optical lightwave signal analyzer, which incorporates a broadband photodetector. The equipment allows the calibration of the microwave elements and cables in the setup, and is controled by a computer. The laser was modulated by an external microwave source and the output was passed through an optical isolator to remove spurious reflections. The dc bias current level was provided by a T bias, while the modulation frequency was swept up to 18 GHz at intervals of 22.5 MHz steps with constant power.

III. Results and discussion

Fig. 1 presents a series of measurements of the optical modulation response with increasing dc bias current in the laser device. The frequency response increases with the optical emitted power, and the 3dB modulation bandwidth achieved at the highest bias current exceeds the 18 GHz range of the experimental setup, and can easily reach the highest value of 21 GHz reported for compressively strained InGaAs/AlGaInAs/InP MQW laser devices [7]. However, the response curves show a characteristic low pass roll-off at higher frequencies that can be attributed to parasitic elements of the laser buried structure. These include the series resistance R and the total capacitance C, which includes the shunt and diffusion capacitances, as well as the device mounting [9]. Carrier transport effects in the SCH waveguiding layers have also been shown to contribute to the low pass frequency roll-off [10]. Nevertheless, the rather high series resistance measured on these devices, in the range 10-20 Ω, suggests that the modulation bandwidth is possibly limited by the parasitic frequency $1/2\pi RC$. A plausible reason for the large series resistance is the highly resistive p-type AlInAs buffer layer.

The analytical expression for the modulation response is obtained from the coupled nonlinear differential rate equations of charge carriers and photons in the laser cavity, under the small signal analysis approximation. The normalised response transfer function at a fixed bias current level in terms of the modulation frequency f is given by [9]

$$R(f) = R_p(f)\frac{f_r^4}{(f^2 - f_r^2)^2 + \frac{f^2\gamma_d^2}{(2\pi)^2}} \quad (1)$$

where f_r is the relaxation oscillation frequency and γ_d is the damping rate. $R_p(f)$ accounts for the parasitic responses.

In order to extract the intrinsic modulation response of the laser device, we have performed the subtraction method described in ref.[11]. This technique eliminates all parasitic contributions to the frequency response that do not vary with the bias current level. The intrinsic response at a given bias current is obtained by performing the logarithmic subtraction of the measured modulation response by the measured response at a lower bias current level. From equation (1), we obtain the logarithmic subtraction of the modulation response function as [11]

$$Sub_{(i-1)} = 10\log\left[\frac{f_{ri}^4}{(f^2 - f_{ri}^2)^2 + \frac{\gamma_{di}^2 f^2}{(2\pi)^2}} \times \frac{(f^2 - f_{r1}^2)^2 + \frac{\gamma_{d1}^2 f^2}{(2\pi)^2}}{f_{r1}^4}\right] \quad (2)$$

where f_{ri}, f_{r1}, γ_{di} and γ_{d1} are the resonance frequency and damping rate at the bias current i and at the lower bias current 1, respectively. Equation (2) can be more easily fitted with the measured modulation response, because all parasitic constant contributions with the current bias level are discarded. Fig. 2 presents the logarithmic subtraction of the data shown in figure 1 by the response function measured at the lowest bias current level. The curve fits obtained using equation (2) are also shown, indicating good agreement with the experimental data. The f_{ri} and γ_{di} data obtained at each bias level are plotted in Figs. 3 and 4, respectively, where f_{r1} and γ_{d1} represent the smallest values. Similar results were also measured on other laser devices. The f_{ri} and g_{di} values measured at lower bias currents are consistent with relative intensity noise measurements performed on the same laser device. The slope of f_r^2 as a function of the bias current is an important factor for high speed applications. The value of 5.69 $\mathrm{GHz}^2/\mathrm{mA}$ obtained for the slope shown in Fig. 3 is larger than data previously reported on lattice matched [12] as well as strained [13,14] index coupled DFB-MQW lasers without facet coatings and fabricated with the InGaAs/InGaAsP/InP material system.

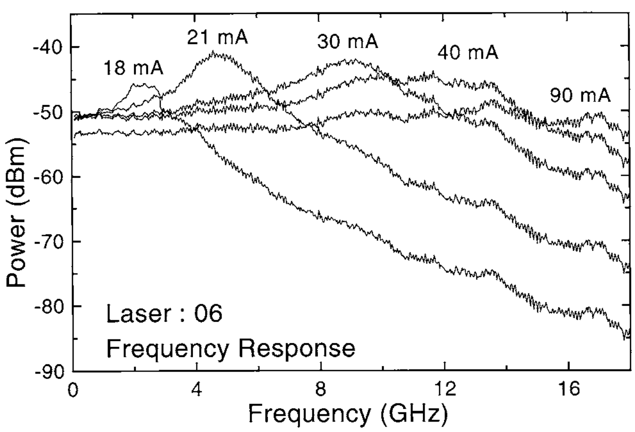

Figure 1: Small signal frequency response measurements of a 1.55 μm DFB-MQW laser at various bias current levels.

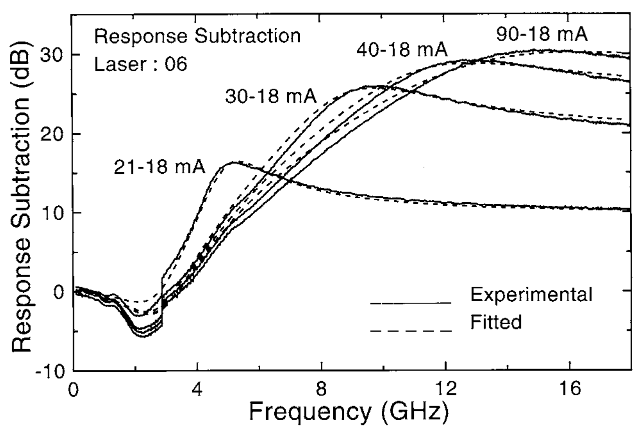

Figure 2. Frequency response subtraction by the modulation response at the lowest current bias level for the data shown in figure 1 (solid curves), and fitted with equation (2) (dotted curves).

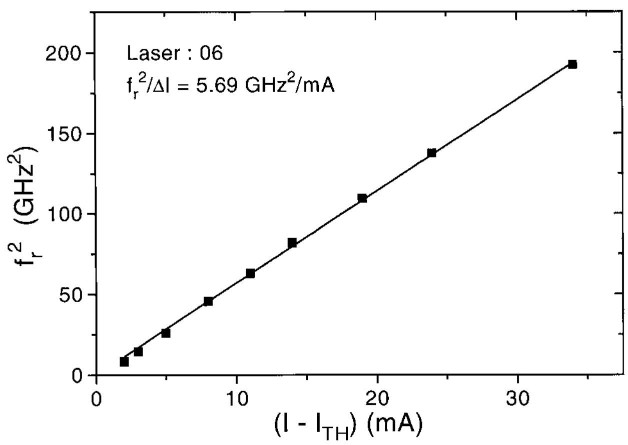

Figure 3. Relaxation oscillation frequency squared versus bias current level above threshold with linear fit.

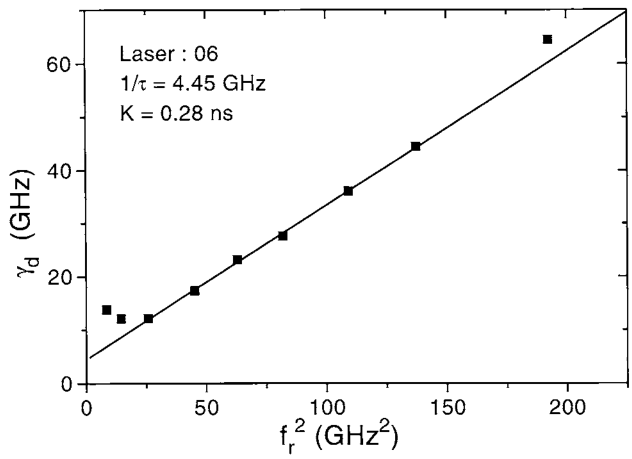

Figure 4. Damping rate versus relaxation oscillation frequency squared with linear fit.

The differential gain dg/dn is obtained with the following relation [15]

$$\frac{dg}{dn} = \frac{(2\pi)^2 eV}{\nu_g \eta_i \Gamma} \left(\frac{f_r^2}{I - I_{th}} \right) \qquad (3)$$

where e is the elementary charge, V is the volume of the active region, ν_g is the group velocity, η_i is the internal efficiency, Γ is the optical confinement factor, I and I_{th} are the bias current at level i and at threshold, respectively. $V = N_Z L_Z L w$, where N_Z is the number of QW layers, L_Z is the QW thickness, L is the cavity length and w is the stripe width. The confinement factor is given by the simple formula $\Gamma = 2 \times 10^{-4} N_Z L_Z$ [16], where L_Z is expressed in Å, and $\nu_g = 7.5 \times 10^9$ cm/s [17].

On the other hand, from the slope of γ_d as a function of f_r^2, one obtains the K factor from the equation [15]

$$\gamma_d = K f_r^2 + \frac{1}{\tau_e} \qquad (4)$$

τ_e is the carrier lifetime and K is related to the nonlinear gain coefficient ϵ by the expression [15]

$$\epsilon = \left(\frac{\nu_g K}{4\pi^2} - \frac{1}{\alpha_i + \alpha_m} \right) \frac{dg}{dn} \qquad (5)$$

where α_i and α_m are the internal and mirror losses, respectively. Finally, the maximum 3 dB frequency bandwidth is obtained from the relation [9]

$$f_{3dB} = \frac{2\pi\sqrt{2}}{K} \qquad (6)$$

In table 1 we have gathered the results of dg/dn, K, ϵ and f_{3dB} obtained with equations (3)-(6) for three laser devices. The values of the MQW laser constants used in the calculations are: $V = 7.2 \times 10^{-12}$ cm^3, $\Gamma = 0.06$, $\eta_i = 1$, $\alpha_i = 30$ cm^{-1} and $\alpha_m = 60$ cm^{-1}. The values of η_i and α_i were determined from measurements of the external efficiency as a function of L. Finally, α_m is defined as $(1/L)\ln(1/R)$, where R is the mirror reflectivity and equals 0.3 for cleaved facets.

Table 1: Intrinsic MQW laser parameters determined from the small signal modulation response.

Laser	dg/dn ($\times 10^{-16}$ cm^2)	K (ns)	ϵ ($\times 10^{-17}$ cm^3)	f_{3dB} (GHz)
06	5.75	0.28	1.32	31.7
09	6.65	0.27	1.52	32.9
13	5.83	0.28	1.34	31.7

The results shown for the intrinsic laser parameters in table 1 are consistent with other high speed data obtained for MQW lasers in the 1.55 μm emission wavelength range. There is little work reported for the compressively strained InGaAs/AlGaInAs/InP material system. A somewhat higher dg/dn value was reported using relative intensity noise measurements with a device having a greater cavity length, but the data was evaluated only at lower f_r values below 10 GHz [6]. Besides, ϵ data is scarce in this material system and has been reported only for lattice matched MQW lasers, where the data diverge, since it is either a factor of 2 - 3 smaller [18], similar [19] or greater [5] than our results shown on table 1. Therefore, the effect of the compressive strain on ϵ remains unclear in InGaAs/AlGaInAs/InP MQW heterostructures. Moreover, the increase of ϵ with the conduction band discontinuity reported in ref.[5] cannot be confirmed, although the conduction band discontinuity increases under compressive strain. On the other hand, we can also compare our data with results reported for the strained InGaAs/InGaAsP/InP material system. In this case, higher values of dg/dn and ϵ have been reported resulting in similar values for K, which imply similar maximum frequency bandwidths f_{3dB} [20,21].

When carrier transport effects in the SCH layers are taken into account, f_{3dB} has been shown to decrease and equation (6) becomes unaccurate [22]. The asymmetric SCH layers of our MQW devices were designed to avoid such effects, but carrier transport in the barrier layers might also contribute to decrease somewhat the measured value for f_{3dB} [23]. However, we should point out that the frequency bandwidth around 20 GHz measured in our laser devices, results mainly from the parasitic response of the device buried structure. These arise from the large series resistance measured on these devices and from leakage currents outside the active region, which degrade the light-current characteristics at higher bias current levels. The latter cannot be eliminated by the logarithmic subtraction of the frequency response described above. Leakage currents through semi-insulating InP:Fe layers are usually explained in terms of double carrier injection [24], which increase the diffusion capacitance at higher bias current levels, and therefore lowers the parasitic frequency $1/2\pi RC$ of the device. Besides, the existence of currents through the laser electrodes, that do not contribute to the stimulated emission, can produce an apparent decrease of the value measured for dg/dn, as shown in a separate work [25]. This might explain the lower dg/dn values measured on our devices compared to results reported for InGaAs/InGaAsP/InP MQW lasers [20,25], though the frequency response measurements for the latter were reported using longer cavity lengths and stripe widths, which increase the active volume, and consequently, increase dg/dn according to equation (3).

IV. Conclusion

We have characterized the high frequency response of compressively strained InGaAs/AlGaInAs/InP DFB-MQW lasers processed with the mushroom stripe buried structure and emitting at the wavelength of 1.55 μm. The frequency response subtraction method was employed to extract the intrinsic response of the MQW active layer under small signal modulation to eliminate the parasitic contributions of the laser structure. The differential gain and the nonlinear gain coefficient of the MQW laser devices were measured, and from the value of K, we have estimated a f_{3dB} above 30 GHz. However, the measured modulation bandwidth is lowered by the low pass frequency roll-off caused by the parasitic response of the laser buried structure, which is produced by the highly resistive AlInAs buffer layer and the leakage currents through the InP:Fe semi-insulating layers.

References

1. E.P. O'Reilly and A.R. Adams, IEEE J. Quantum Electron. **30**, 366 (1994).
2. S. Seki, T. Yamanka, W. Lui and K. Yokoyama, J. Appl. Phys. **75**, 1299 (1994).
3. M.T. Furtado, W. Carvalho Jr., C.M.A. Coghi, E.J.T. Manganote and A.C.G. Bordeaux-Rêgo, Rev. Bras. Fis. Apl. Instr., in press.
4. M. Ishikawa, R. Nagarajan, T. Fukushima, J.G. Wasserbauer and J.E. Bowers, IEEE J. Quantum Electron. **28**, 2230 (1992).
5. A. Wakatsuki, Y. Kawamura, Y. Noguchi and H. Iwamura, IEEE Photon. Technol. Lett. **4**, 383 (1993).
6. M.L. Xu, G.L. Tan, J.M. Xu, M. Irikawa, H. Shimizu, T. Fukushima, Y. Hirayama and R.S. Mand, IEEE Photon. Technol. Lett. **7**, 947 (1995).
7. F. Steinhagen, H. Hillmer, R. Losch, W. Schlapp, H. Walter, R. Gobel, E. Kuphal, H.L. Hartnagel

and H. Burkhard, Electron. Lett. **31**, 274 (1995).
8. H. Hillmer, S. Hansmann, H. Burkhard, H. Walter, A. Krost and D. Bimberg, IEEE J. Quantum Electron. **30**, 2251 (1994).
9. R. Olshanski, P. Hill, V. Lanzisera and W. Powazinik, IEEE J. Quantum Electron. **23**, 1410 (1987).
10. R. Nagarajan, T. Fukushima, S.W. Corzine and J.E. Bowers, Appl. Phys. Lett. **59**, 1835 (1991).
11. P.A. Morton, T. Tanbun-Ek, R.A. Logan, A.M. Sergent, P.F. Sciortino Jr. and D.L. Coblentz, IEEE Photon. Technol. Lett. **4**, 133 (1992).
12. K. Uomi, M. Aoki, T. Tsuchiya, M. Suzuki and N. Chinone, IEEE Photon. Technol. Lett. **3**, 493 (1991).
13. H. Lu, G.P. Li and T. Makino, IEEE Photon. Technol. Lett. **5**, 861 (1993).
14. N. Otsuka, M. Kito, M. Ishino and Y. Matsui, IEEE J. Quantum Electron. **32**, 1230 (1996).
15. J.D. Ralston, S. Weisser, I. Esquivias, E.C. Larkins, J. Rosenzweig, P.J. Tasker and J. Fleissner, IEEE J. Quantum Electron. **29**, 1648 (1993).
16. J.P. Loehr and J. Singh, IEEE J. Quantum Electron. **27**, 708 (1991).
17. D. McDonald and R.F. O'Dowd, IEEE J. Quantum Electron. **31**, 1927 (1995).
18. A. Grabmaier, A. Hangleiter, G. Fuchs, J.E.A. Whiteaway and R.W. Glew, Appl. Phys. Lett. **59**, 3024 (1991).
19. F. Girardin, G.H. Duan, C. Chabran, P. Gaillon, M. Blez and M. Allovon, IEEE Photon. Technol. Lett. **6**, 894 (1994).
20. A.P. Wright, A.T.R. Briggs, A.D. Smith, R.S. Baulcomb and K.J. Warbrick, Electron. Lett. **29**, 1848 (1993).
21. H. Lu, T. Makino and G.P. Li, IEEE J. Quantum Electron. **31**, 1443 (1995).
22. R. Nagarajan, M. Ishikawa and J.E. Bowers, Electron. Lett. **28**, 846 (1992).
23. Y. Chen, M.S. Wartak, H. Lu and T. Makino, J. Appl. Phys. **78**, 5515 (1995).
24. S. Asada, S. Sugou, K. Kasahara and S. Kumashiro, IEEE J. Quantum Electron. **25**, 1362 (1989).
25. M.T. Furtado, W. Carvalho Jr., A.M. Machado and K. Jomori, Braz. J. Phys., in press.